Synthesis of ZIF-94 from Recycled Mother Liquors: Study of the Influence of Its Loading on Postcombustion CO$_2$ Capture with Pebax Based Mixed Matrix Membranes

Md Rafiul Hasan, Lorena Paseta, Magdalena Malankowska, Carlos Téllez, and Joaquín Coronas**

Global energy demand is met in large part, by burning of fossil fuels, which is causing global warming. Mixed matrix membranes (MMMs) with metal organic frameworks (MOFs) as fillers are an interesting alternative for capturing post combustion CO$_2$ which would make the energy sector sustainable. This research is focused on the synthesis of MOF ZIF-94 from the recycling of its mother liquors and the incorporation of synthesized MOF into a Pebax MH 1657 for MMM fabrication. The pH and the temperature of ZIF-94 synthesis are modified and monitored and this results in various nanoparticle diameters (average particle size in the range of 41 ± 8–180 ± 73 nm). Incorporation of ZIF-94 significantly improves the performance of the bare Pebax MH 1657 membrane. The maximum CO$_2$/N$_2$ selectivity and CO$_2$ permeability are obtained for 10 wt% ZIF-94 loading in 9 wt% (polymer concentration in 70/30 (v/v) ethanol/water solution) Pebax MH 1657 matrix being 36 ± 7 (71% increment compared to bare membrane) and 137 ± 31 Barrer (80% improvement), respectively.

1. Introduction

Fossil fuels are considered as the primary energy sources in anthropogenic activities according to the International Energy Agency, and it is estimated that the global energy demand will increase by substantial amount by the year 2030.[1] Burning fossil fuels produces huge CO$_2$ emission to the environment with 6% increment every year[2] causing global warming

M. R. Hasan, L. Paseta, M. Malankowska, C. Téllez, J. Coronas
Instituto de Nanociencia y Materiales de Aragón (INMA)
CSIC-Universidad de Zaragoza
Zaragoza 50018, Spain
E-mail: magnal@unizar.es; coronas@unizar.es
M. R. Hasan, L. Paseta, M. Malankowska, C. Téllez, J. Coronas
Chemical and Environmental Engineering Department
Universidad de Zaragoza
Zaragoza 50018, Spain
M. R. Hasan
Department of Chemical Engineering
Jashore University of Science and Technology
Jashore 7408, Bangladesh

and unpredictable climatic changes such as rising sea levels, melting of glaciers throughout the entire planet[2] and affecting agriculture,[3] to name a few.

A release of greenhouse gases will continue if no action is taken either for searching of green energy sources or filtering postcombustion gases to limit the global temperature rise below 2 °C (which was established during Paris conference in 2015).[4] Carbon capture and storage (CCS) is one of the methods of purification of flue gas after capturing CO$_2$ being a straightforward solution to avoid concerned challenges. There are several possible technologies for CCS either based on solvents (absorption), solid adsorbents (adsorption), cryogenic process or membrane-based approach. Even though chemical solvent treatment (especially by amines), physical absorption, and cryogenic separation are very effective methods, they are characterized by high vapor pressure and emission of toxic compounds. Moreover, it is very difficult to recycle them mainly due to the high reaction heat.[2,5]

Membrane-based technology, a fast growing and environmental-friendly separation process, has the potential to replace conventional energy-intensive technologies and provides reliable solutions for CCS. This is mainly due to the low energy consumption linked to membranes, operation flexibility and simplicity, good stability, easy control and scale-up. Typically, polymeric membranes are used for the gas separation thanks to a solution–diffusion mechanism that benefits from the intrinsic property of the material for the gas transport. However, such membranes are bounded by their performance, known as the Robeson upper bound,[6] where gas permeability is sacrificed for gas mixture selectivity and vice versa. Moreover, higher membrane surface area is required for the expected separation to be industrially attractive.

A class of polymeric composite membranes named mixed matrix membranes (MMMs) with specific fillers coupled with other existing processes (cryogenic/absorption) could be the best technology for CO$_2$ capture. MMMs are made of a base polymeric matrix and a compatible inorganic micro/nanosized filler that is integrated inside the micropores of polymeric materials to improve their properties.[7] In fact, the filler contributes to favor the permeability of the desired component in the mixture through the modification of the diffusivity and solubility

**ADVANCED
SCIENCE NEWS**
www.advancedsciencenews.com

**ADVANCED
SUSTAINABLE
SYSTEMS**
www.advsustainsys.com

properties of the membranes. In consequence, permeability of gases through MMMs depends on intrinsic compatibility between polymer-filler pair, confirmed by proper selection of organic matrix and inorganic filler.

Metal organic frameworks (MOFs) are promising MMM fillers that constitute a growing class of crystalline and porous (porosity of around 90%) materials presenting combined properties of inorganic (metal ions as cluster) and organic (linker) materials often characterized by high specific surface area (beyond 6000 m^2 g^{-1}).[7] MOFs are found to be used in a wide range of applications, such as capture and storage of gas for clean energy, membrane separation, and catalysis to name a few.[8] CO_2 capture from flue gas with MOFs is the cutting-edge research field in the recent years. Zeolite imidazolate frameworks (ZIFs) are some of the most studied MOFs, since their crystal structure sustain even a boiling point temperature of a solvent (benzene and water).[9] ZIFs exhibit a zeolite type structure and they are characterized by exceptional chemical and thermal stability (up to 400 °C), high microporosity (with micropores in the 0.3–0.5 nm range), and large specific surface area. They are composed of a divalent metal cation (i.e., Co^{2+} or Zn^{2+}) that is linked to nitrogen atoms which are part of a deprotonated imidazole molecule creating tetrahedral frameworks.

ZIF-94, also known as SIM-1,[10–12] possesses an SOD topology along with well distributed and defined 3D pore networks.[13] It possesses a high CO_2 adsorption capacity of 2.4 mmol g^{-1} at 1 bar and 25 °C with limiting pore diameter of 2.6 Å and cavity diameter 9.6 Å[12,14] compared to other typical ZIFs for the same application (ZIF-8 (0.7–0.8 mmol g^{-1}, 3.4 Å limiting pore diameter and 11.4 Å cavity diameter),[15,16] ZIF-7 (1.6 mmol g^{-1}, 2.9 Å limiting pore diameter and 7.5 Å cavity diameter), ZIF-93 (1.7 mmol g^{-1} and 17.9 Å cavity diameter), and ZIF-11 (0.8 mmol g^{-1}, 3.0 Å limiting pore diameter and 14.9 Å cavity diameter)) at 1 bar operating pressure and 25 °C.[17–19] Morris et al. have demonstrated that ZIF-94 shows superior uptake of CO_2 up to 3 bar when compared with ZIF-7, ZIF-93, and ZIF-11.[12] This outperformance of ZIF-94 in terms of CO_2 absorption results from the combination of its SOD topology, flexible pore opening, and aldehyde functional group of its ligand. In a typical ZIF-94 synthesis, if the crystallization yield is below 100%, the mother liquor contains unreacted metal and ligand, together with the solvent (e.g., MeOH). All these reagents are expensive to replace and usually are discarded after the synthesis. Hence, it is important to investigate a reagent recycling on the synthesis of MOFs considering environmental and economic reasons.[20,21] Few works have been developed dealing with this issue with the example of ZIF-8.[21–24] In these research articles, the attempts to synthesize ZIF-8 from recycled mother liquors are related to the use of sodium hydroxide and potassium hydroxide as well as ammonia as deprotonators to initiate the nucleation and to favor the crystal growth.[25,26]

As has been commented, ZIFs have been widely used as additives in mixed matrix membranes to improve the separation properties of membranes,[27,28] examples include some cases, with ZIF-94 as filler.[14,17] The use as fillers of ZIFs and in general of MOFs synthesized with mother liquors is to be explored in depth.

The objective of this research is to synthesize ZIF-94 from recycled mother liquors emphasizing the influence of different parameters (such as pH or temperature) on the final MOF structure, and to use it as a filler to be incorporated in Pebax MH 1657 for postcombustion CO_2 capture. Pebax MH 1657 (polyamide-*b*-ethylene oxide, or commercially known as Pebax) is a commercial rubbery and thermoplastic polymer that is very attractive especially for polar gas separation, such as CO_2, from nonpolar light gases, such as N_2. The effects of recycled MOF loading and polymer concentration in the casting solution were investigated, as well as the influence of using filler synthesized from the mother liquor and by the original method.
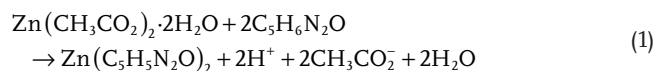
2. Experimental Section

2.1. Materials

Zinc acetate dihydrate and 4-methyl-5-imidazolecarboxaldehyde were purchased from Acros Chemicals (98% and 99% purity, respectively). Methanol (99.8%) was obtained from Honeywell, and anhydrous tetrahydrofuran (THF, ≥99.9%) was obtained from Sigma-Aldrich. Sodium hydroxide (NaOH pellets, ACS grade) was purchased from Carlo Erba. Absolute ethanol was purchased from Gilca, Spain. For the membrane fabrication, commercially available Pebax MH 1657 was kindly provided by Arkema, France.

2.2. Methodology

2.2.1. Original Synthesis of ZIF-94

ZIF-94 was synthesized by a two-step process according to Madhav et al.[29] that in turn resulted from the modified procedure of Johnson et al.[30] 1) Initially, the required amount of zinc acetate dihydrate (7.2 mmol) together with the required amount of NaOH (14.4 mmol) was dissolved in 6 mL of methanol (MeOH), and 2) the proportional amount of 4-methyl-5-imidazole carboxaldehyde (14.4 mmol) was dissolved in 15 mL of THF. Next, the MeOH solution was added to the THF solution under vigorous stirring. Afterward, the mixture was stirred for 16 h at room temperature (RT). The product was collected by centrifugation at 10 000 rpm for 10 min and washed with MeOH under the same conditions (the process was repeated three times). After, ZIF-94 nanocrystals were activated by refluxing with 50 mL of MeOH/g ZIF-94 for 1.5 h and collected by centrifugation at 10 000 rpm for 10 min. The resulting ZIF-94 was dried overnight at RT. Schematic representation of the synthesis of ZIF-94 is shown in **Figure 1**. A summary of the reagents used for ZIF-94 synthesis with their molar ratios are represented in Table S1 of the Supporting Information.

The representative reaction for the synthesis of ZIF-94 is shown below in Equation (1) ($C_5H_6N_2O$ being 4-methyl-5-imidazolecarboxaldehyde). Two moles of acetic acid are produced per mol of ZIF-94, justifying the need of the addition of base as a means to control the pH of the reaction
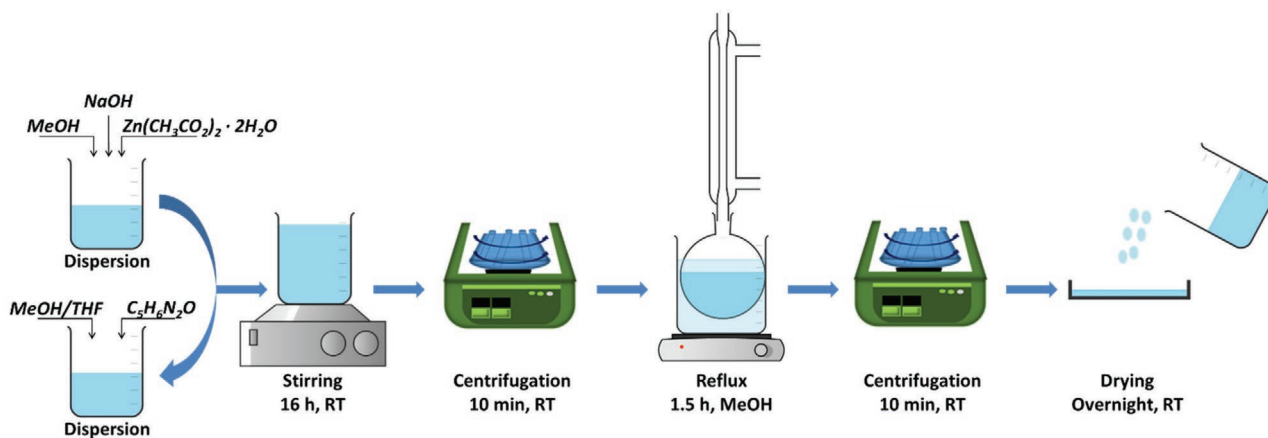
$$Zn(CH_3CO_2)_2 \cdot 2H_2O + 2C_5H_6N_2O \rightarrow Zn(C_5H_5N_2O)_2 + 2H^+ + 2CH_3CO_2^- + 2H_2O \tag{1}$$

**ADVANCED
SCIENCE NEWS**
www.advancedsciencenews.com

**ADVANCED
SUSTAINABLE
SYSTEMS**
www.advsustainsys.com

Figure 1. Sketch of synthesis of MOF ZIF-94.

The Scherrer equation (Equation (2)) was used to calculate primary ZIF-94 particle sizes from X-ray diffraction (XRD) patterns

$$L = \frac{K \cdot \lambda}{B \cdot \cos\theta} \tag{2}$$

where L is the crystallite size (nm), K is a constant (0.96), λ is X-ray wavelength, B is the peak width, and θ is the diffraction angle.

Moreover, the yield of the reaction was defined as the ratio of the amount of solid ZIF-94 obtained from 100 g of synthesis mixture to the maximum possible amount of ZIF-94 that can be produced from 100 g of synthesis mixture if all limiting reactants (Zn^{2+} or ligand, both in stoichiometric quantity) are consumed according to the equation below

$$\text{Yield}\,(\%) = \frac{\text{Exp. ZIF} - 94}{\text{Theor. ZIF} - 94} \times 100 \tag{3}$$

where Exp. ZIF-94 is the mass of dry ZIF-94 collected after the synthesis and Theor. ZIF-94 is the theoretic yield considering the limiting reagent and the empirical formula of ZIF-94, $Zn(C_5H_5N_2O)_2$.

2.2.2. Synthesis of ZIF-94 Crystals from Recycled Mother Liquors

After the synthesis of ZIF-94, the mother liquor was separated by centrifugation from the nanocrystals to be used in the subsequent synthesis of ZIF-94. The main purpose was to keep the size and the morphology of the nanocrystals as similar as possible to the original ZIF-94 reproducing the exact same synthesis. To do that, once synthesized the nanocrystals were recovered by centrifugation, and thermogravimetry was used to estimate the percentage of pure ZIF-94 synthesized (i.e., excluding trapped solvent and ligand). Knowing this percentage, the quantities of the unreacted reagents on the mother liquor were calculated by mass balance and the lacking amounts of those reagents were added together with the volume of loss solvent. The reaction produces acetic acid (see Equation (1)), therefore the pH of the medium decreases with the crystallization.

In order to restore the pH of the mother liquor and to favor the deprotonation of the organic ligand, a procedure of adding NaOH as a base was conducted.[29] Besides, some experiments were carried out changing the pH or the temperature of the original synthesis to observe how these parameters affect the crystallinity, morphology, and particle size of ZIF-94. Such procedure resulted in the formation of products A.1–A.5 for the pH control and product B for the temperature control. **Figure 2** shows a scheme of different synthesis procedures conducted in this study.

2.2.3. Fabrication of MMMs

MMMs were fabricated with two different polymer concentrations: 6 and 9 wt% Pebax MH 1657 as a matrix (i.e., the polymer concentration in the solvent as a casting solution) and various ZIF-94 doses (5–20 wt%). The MMMs were prepared following a two-step process.[31] First, 6 and 9 wt% Pebax MH 1657 (of total weight of 3 g (polymer + solvent)) was dissolved in EtOH/water (70/30 (v/v)) by stirring under reflux for 1 h. Afterward, the dissolved polymer was used to cast bare polymeric membranes. In case of MMMs fabrication process, ZIF-94 was dispersed in the dissolved polymer. The required amount of filler (5–25 wt%) which was calculated against the amount of Pebax MH 1657 being used, was dispersed in 1.5 mL of EtOH/water (70/30) by repeated sonication and stirring at RT for 1 h. Next, both dispersions were mixed and kept stirred at RT overnight. In the extension of the fabrication process, the solution was poured on a Petri dish. At the end of the process, the membranes were dried for 48 h in a top-drilled box under a solvent-saturated atmosphere at environmental conditions.

2.3. Characterization

The morphology of synthesized ZIF-94, as well as surface and cross-sectional morphologies of Pebax MH 1657 bare membrane and its MMMs were inspected by scanning electron microscopy (SEM) with back scattered electron mode using an Inspect F50 model scanning microscope (FEI), operated at 10 kV. Additionally,
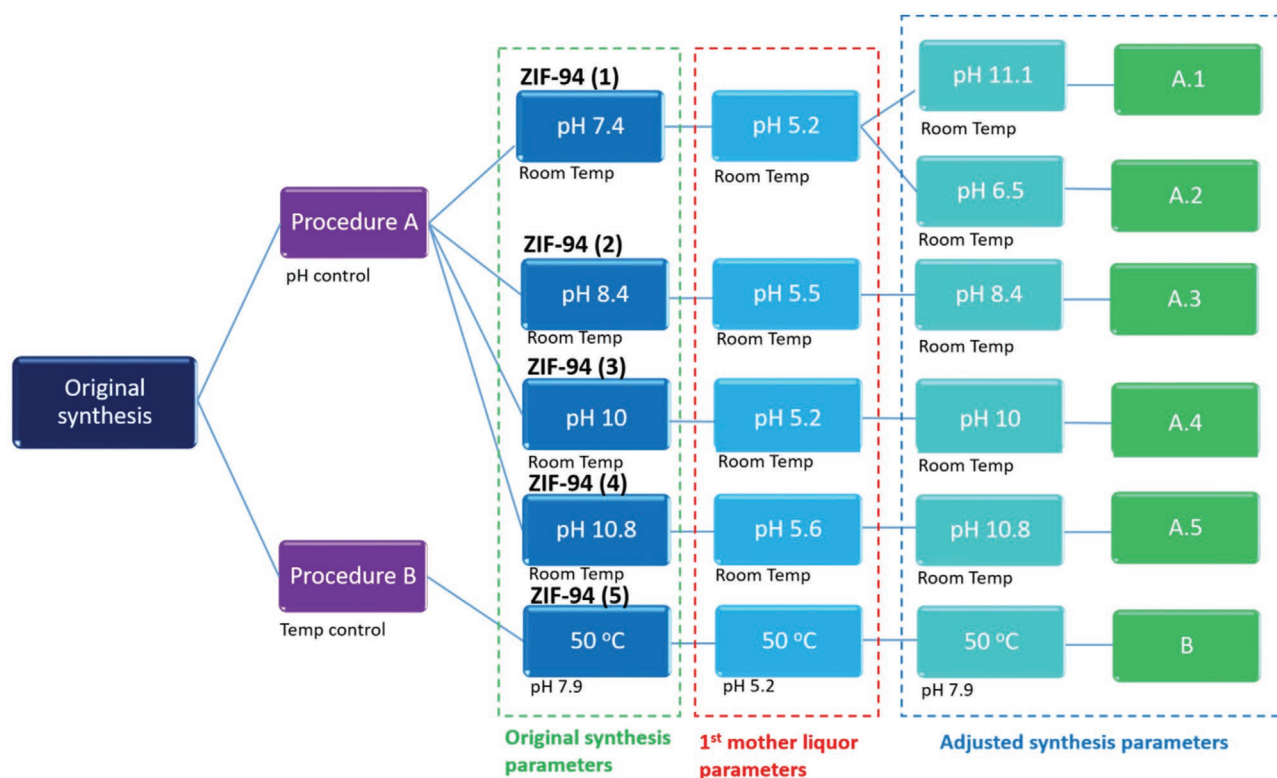
Figure 2. Schematic representation of all syntheses carried out. The washing was performed in refluxing MeOH followed by drying at room temperature.

the images were further analyzed using ImageJ software to analyze particle size distribution of the materials under investigation. Transmission electron microscopy (TEM) was carried out to examine the morphology of ZIF-94 synthesized from the recycled mother liquors. The sample was placed on a carbon mesh grid and observed under an FEI Tecnai T20 transmission electron microscope operated at 200 kV. Thermogravimetric analysis (TGA) was carried out using a Mettler Toledo TGA/STDA 851e. Small pieces of membranes as well as ZIF-94 in the form of a powder ($\approx$5 mg) were placed in 70 μL alumina pans that were heated under an air flow (40 mL (STP) min^{-1}) from 35 to 700 °C at a heating rate of 10 °C min^{-1}. Loss of weight as a function of temperature is revealed from TGA analysis which is characteristic of removal of solvents and thermal degradation of the sample under investigation. The N$_2$ adsorption–desorption isotherms were obtained using Micromeritics Tristar 3000 at 77 K. Before these measurements, the samples were degassed for 8 h under vacuum at 200 ° using a heating rate of 10 °C min^{-1}. Brunauer-Emmett-Teller (BET) analysis provides specific surface area of porous materials. Membranes and nanoparticles were also characterized by XRD using a Panalytical Empyrean equipment with Cu Kα radiation (λ = 0.154 nm), over the range of 5°–40° at a scan rate of 0.03° s^{-1}, to examine the *d*-spacing of the nanoparticles and membranes.

2.4. Gas Separation Measurements

The permeation of gases through polymeric membranes is frequently explained by the solution–diffusion mechanism where the performance will depend on the polymer intrinsic properties toward each of the gas types (i.e., CO$_2$, N$_2$, etc.) such as solubility and diffusivity.[32] Based on this mechanism, the performance of the membranes is determined by the permeability, which is the product of solubility by diffusion, and the selectivity, which is the ratio of the permeability of the gases to be separated. The separation of the CO$_2$/N$_2$ mixture was performed in the experimental system that is schematically presented in **Figure 3**. The membranes were cut and placed in a module consisting of two stainless steel pieces and a 316LSS macroporous disk support (Mott Co.) with a 20 μm nominal pore size. Membranes, 2.12 cm^2 in area, were gripped inside with Viton O-rings. To control the temperature of the experiment, which influences gas separation, the permeation module was placed in an UNE 200 Memmert oven. Gas separation measurements were carried out by feeding the postcombustion gaseous mixture of CO$_2$/N$_2$ (15/85 cm^3 (STP) min^{-1}) at an operating pressure of 3 bar and 35 °C to the feed side, controlled by two mass-flow controllers (Alicat Scientific, MC-100CCM-D). The permeate side of the membrane was swept with 2 cm^3 (STP) min^{-1} of He, at atmospheric pressure ($\approx$1 bar) (Alicat Scientific, MC-5CCM-D). Concentrations of N$_2$ and CO$_2$ in the outgoing streams were analyzed online by an Agilent 3000A microgas chromatograph. Permeability was calculated in Barrer (10^{-10} cm^3 (STP) cm cm^{-2} s^{-1} cm Hg^{-1}) once the steady state of the exit stream was reached (at least after 3 h). The separation selectivity was calculated dividing the permeability of CO$_2$ by that of N$_2$.
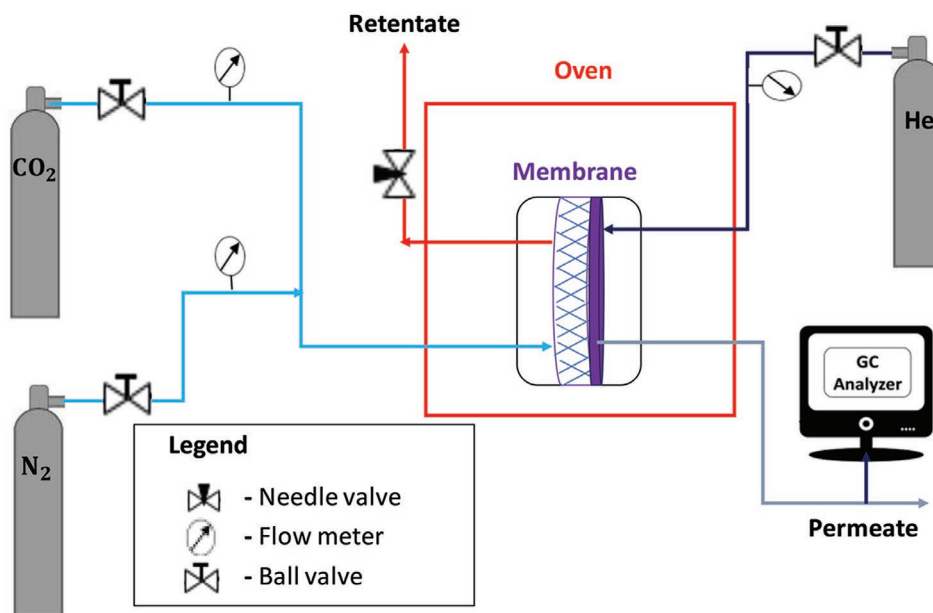
**ADVANCED
SCIENCE NEWS**

www.advancedsciencenews.com

**ADVANCED
SUSTAINABLE
SYSTEMS**

www.advsustainsys.com

Figure 3. Gas permeation experimental system operating at 35 °C.

3. Results and Discussion

3.1. Characterization of ZIF-94 from the Original Synthesis

TEM analysis of the synthesized ZIF-94 particles represented in Figure S1A of the Supporting Information revealed an average particle size of 53 ± 14 nm measured from more defined and clearly not agglomerated particles. This value is in agreement with ≈50 nm value calculated by Scherrer equation (Equation (2)). The reaction yield was ≈71.4% (see Equation (3)).

X-ray diffraction pattern allowed to determine the crystallinity, purity of the product, and its crystal phases. Figure S2 of the Supporting Information represents the XRD pattern of the synthesized ZIF-94 where relative intensities and peak positions match well with published crystallographic data corresponding to ZIF-8 (since the two MOFs share the same SOD structure).[12,17,33] The N_2 adsorption–desorption analysis provides BET specific surface area (SSA) that lies

in between 415 and 480 m^2 g^{-1} for ZIF-94, according to the literature.[12,34] Synthesized ZIF-94 produced BET SSA of 464 m^2 g^{-1} (see **Table 1**). Moreover, the prescribed MOF shows type I isotherm with additional small hysteresis. This suggests some hierarchical porosity due to the mesoposority present in between MOF nanoparticles.

3.2. Characterization of ZIF-94 Synthesized from Recycled Mother Liquors

3.2.1. pH Control and Modification (Procedure A)

Five different syntheses were conducted in procedure A where the pH was monitored and controlled (see Figure 2 for details of each procedure). In the first case, the initial pH of the original synthesis was equal to 7.4 (ZIF-94 (1) – see Figure 2), which decreased down to 5.2 after 16 h of the reaction due

Table 1. Synthesis pH, yield, BET SSA, and average particle size of ZIF-94 obtained from electronic microscopy images, product A.1, product A.2, ZIF-94 (2), product A.3, ZIF-94 (3), product A.4, ZIF-94 (4), and product A.5 obtained at room temperature. ZIF-94 and ZIF-94 (2) to (4) correspond to fresh reagents syntheses, while Products A.1 to A.5 used recycled mother liquors.

Sample code	Synthesis pH	Yield [%]	BET specific surface area [m^2 g^{-1}]	Average particle diameter [nm]
ZIF-94	7.4	71.4	464	53 ± 14
Product A.1	11.1	41.5	417	49 ± 11
Product A.2	6.5	53.8	428	34 ± 16
ZIF-94 (2)	8.4	84.6	405	37 ± 8
Product A.3		67.5	423	44 ± 34
ZIF-94 (3)	10	77.4	463	43 ± 10
Product A.4		60.5	483	34 ± 14
ZIF-94 (4)	10.8	77.0	442	199 ± 84
Product A.5		61.8	506	36 ± 8

**ADVANCED
SCIENCE NEWS**
www.advancedsciencenews.com

**ADVANCED
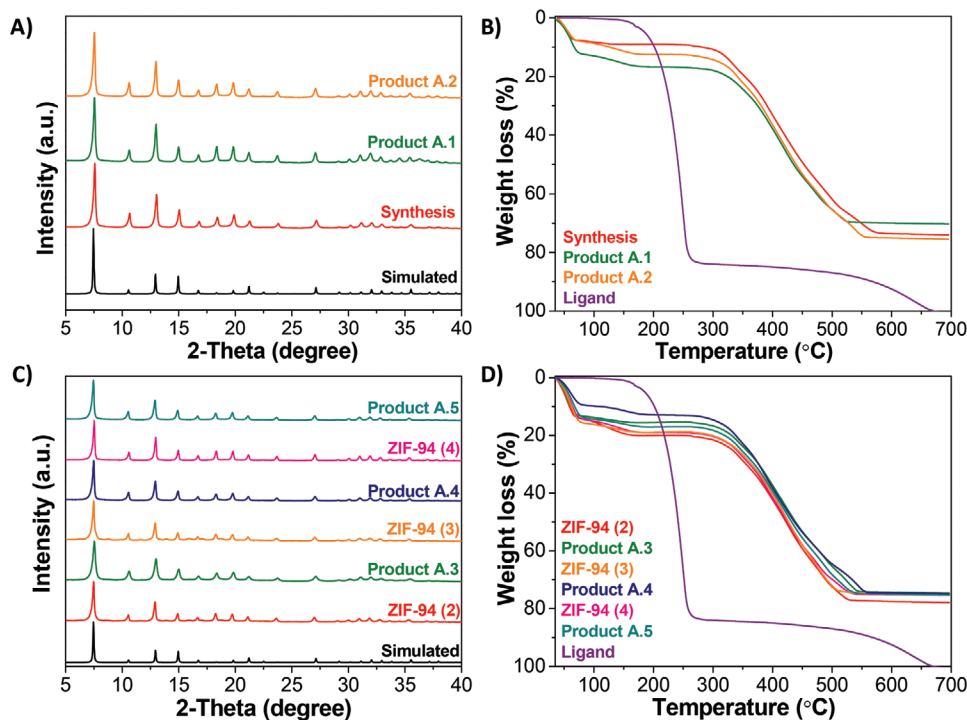SUSTAINABLE
SYSTEMS**
www.advsustainsys.com

Figure 4. ZIF-94 and products A.1 and A.2: A) XRD patterns, and B) TGA curves. ZIF-94 (2), product A.3, ZIF-94 (3), product A.4, ZIF-94 (4), and product A.5. (A) XRD pattern and (B) TGA curves.

to the formation of acetic acid according to Equation (1). All the reactions were carried out a room temperature. As it was mentioned above, NaOH was added to control the influence of pH on the ZIF-94 nanocrystals morphology and size. Two pH values were obtained: 11.1 resulting in product A.1 and 6.5 resulting in product A.2. The obtained products were washed in MeOH under reflux during 1.5 h and dried at RT.

As it can be observed in **Figure** 4A, XRD patterns of products A.1 and A.2 match well with the XRD pattern of the ZIF-94 obtained in the original synthesis. On the other hand, thermogravimetric analysis (Figure 4B) shows two weight losses between 35 and 180 °C corresponding to the removal of MeOH and THF used in the synthesis. Besides, neither the ZIF-94 obtained from the original synthesis nor products A.1 and A.2 have organic ligand trapped in the structural pores. The yield of the reactions was calculated according to Equation (3) being higher for product A.2 (53.8%) than for product A.1 (41.5%), although in both cases, the yield was lower compared to the ZIF-94 from the original synthesis (71.4%). Moreover, the BET SSA decreased slightly for both products being equal to 417 and 428 m^2 g^{-1} for product A.1 and A.2, respectively (see Table 1), in comparison to that of the original synthesis (464 m^2 g^{-1}). Nevertheless, the values are still within those reported in literature (415–480 m^2 g^{-1}).[12,34] The average particle sizes of both products were determined from TEM images by measuring ≈80 particles of each sample and calculating the average value. In case of product A.1, its particle size was 49 ± 11 nm, whereas for product A.2 it was equal to 34 ± 16 nm. In addition, product A.1 was characterized by higher particle agglomeration than product A.2, and large particles coexisted with typical nanoparticles. The calculations done with Scherrer equation

(Equation (2)) revealed that the particle sizes should be in the range of 40–42 nm which reinforced the idea about the small formation of ZIF-94 agglomerates in the case of product A.1 in line with the hysteresis loops observed in the adsorption and desorption isotherms (see Figure S3, Supporting Information).

Next, the reactions with pH equal to 8.4, 10, and 10.8 of the original syntheses (labeled as ZIF-94 (2), ZIF-94 (3), and ZIF-94 (4)) were conducted to obtain their corresponding products (A.3, A.4, and A.5, respectively). The washing and drying procedures were the same as it was described in case of products A.1 and A.2. As Figure 4C shows, the XRD patterns of all synthesized materials are consisted with the ZIF-94 simulated pattern. The decomposition temperature of all materials is in agreement with that of ZIF-94 (≈270 °C) and no weight loss due to the organic ligand trapped in the pores is observed (Figure 4D). Nonetheless, two weight losses appear between 35 and 180 °C due to the removal of MeOH and THF used in the synthesis as it was in case of products A.1 and A.2.

As it is shown in Table 1, the highest yield was obtained when the initial synthesis and the synthesis from recycled mother liquor were performed at pH = 8.4 (67.5%, product A.3). However, their BET SSA values were the smallest compared to those of the other samples, these values being still in the range of those published in the literature (415–480 m^2 g^{-1}).[12,34] Regarding the samples obtained at pH = 10 (product A.4) and 10.8 (product A.5), their yields (60.5% and 61.8%, respectively) were slightly lower than the one obtained in the original synthesis (71.4%). The same happens with their corresponding BET SSA values.

Figure S4 of the Supporting Information shows the TEM images of the materials obtained at different pH values and their corresponding products from the recycled mother liquors
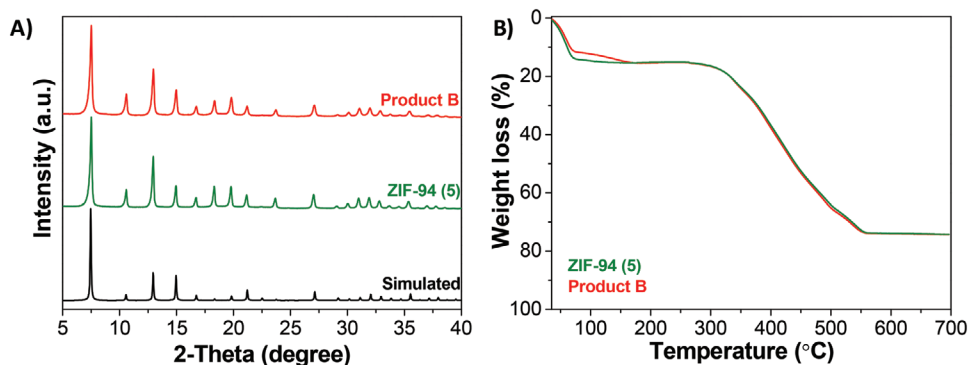
Figure 5. ZIF-94 (5) and product B. A) XRD patterns and B) TGA curves.

(products A.3–A.5). As can be observed, ZIF-94 synthesized at pH = 10.8 has larger particle size in comparison to the previous samples. Moreover, it can also be seen that agglomerates of particles appear in all cases, in line with the calculations done with the Scherrer equation (30–50 nm).

3.2.2. Temperature Control at 50 °C (Procedure B)

As has been said above, one synthesis (ZIF-94 (5)) and its recycle were carried out at 50 °C as a way to investigate the effect of the temperature on the properties of ZIF-94 obtained (product B). The initial pH of the original synthesis was equal to 7.9 and after 16 h of the reaction it decreased down to 5.2 due to the formation of acetic acid. Next, the pH of the mother liquor after the addition of the consumed reactants was increased up to 7.9. **Figure 5** shows the XRD pattern and the TGA curves of the ZIF-94 synthesized at 50 °C and product B obtained from the recycled mother liquor of this synthesis. As can be seen, the peak positions and the intensities of both materials match well with those of the simulated pattern of ZIF-94. Besides, TGA curves do not present any weight loss due to the presence of organic ligand trapped in the pores indicating that the material is well activated.

Table 2 shows the characteristics of the materials obtained when both the initial synthesis and the recycled mother liquor were carried out at 50 °C. The yield obtained was higher than the one obtained in the original synthesis (see Table 1), whereas the BET surface area was closer to the original ZIF-94 (464 m^2 g^{-1}). This allows to think that this reaction is favored with temperature.

The average particle size (180 ± 73 nm) of the original synthesis (ZIF-94 (5)) is much larger than in case of recycled product B (41 ± 8 nm) shown in Table 2 and Figure S5 (Supporting Information). According to the Scherrer equation, the

crystal size of these samples should be in the 41–49 nm range, suggesting the existence of ZIF-94 agglomerates. However, in both cases the yield is higher than in the synthesis of ZIF-94 and its recycle.

For the testing of the synthesized MOFs and the improvement in membrane performance for gas separation after their incorporation in MMMs, four samples were selected: i) freshly synthesized ZIF-94 according to Johnson et al.[30] and particle size of 173 ± 78 nm, ii) ZIF-94 (3) at pH 10, RT and particle size of 43 ± 10 nm, iii) ZIF-94 (5) at pH 7.9, 50 °C and particle size of 180 ± 73 nm, and iv) product B synthesized from the recycled ZIF-94 (5) with particle size of 41 ± 8 nm. The reason for such selection was to examine the effect of different particle size, the influence of the recycled or freshly synthesized MOF and the effect of the particles synthesized either at higher pH or higher temperature on the final performance of the membrane. All the details of the samples chosen for the incorporation in the MMMs are presented in **Table 3**.

3.3. Characterization and Performance of MMMs

3.3.1. MMMs Characterization

The fabricated membranes were thoroughly characterized for homogenous MOF distribution, lack of defects, cracks, and non-selective gaps. **Figures 6**A shows, as an example, an SEM image of one the MMMs: 9 wt% Pebax MH 1657 with 15 wt% ZIF-94 (1) (i.e., the MOF obtained from fresh reactants, see Table 3). ZIF-94 was homogenously distributed across the polymeric matrix, no visible defects can be appreciated ensuring well fabricated membranes. TGA analysis of three different MMMs was also investigated and compared to a bare polymeric membrane

Table 2. Yield, BET SSA, and average particle size of ZIF-94 (5) and product B obtained at 50 °C.

Sample code	Synthesis pH	Yield [%]	BET specific surface area [m^2 g^{-1}]	Average particle diameter [nm]
ZIF-94 (5)	7.9	78.9	457	180 ± 73
Product B	7.9	62.7	468	41 ± 8

Table 3. Different types of fillers used in MMMs for the gas separation analysis.

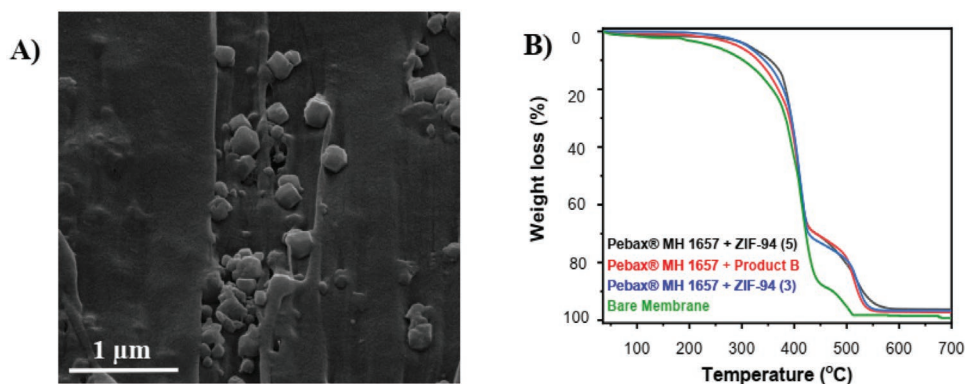| Sample code	Properties of MOF	BET surface area [m^2 g]	Average particle diameter [nm]
ZIF-94 (1)[30]	Original 1st synthesis	317	173 ± 68
ZIF-94 (3)	Fresh synthesis	463	43 ± 10
ZIF-94 (5)	Fresh synthesis	457	180 ± 73
Product B	Recycled from ZIF-94 (5)	468	41 ± 8

Figure 6. A) SEM imaging of a MMM 9 wt% Pebax MH 1657 with 15 wt% ZIF-94 (1) as a filler cross section and B) TGA analysis of the bare Pebax MH 1657 membrane and a comparison to MMMs with different types of fillers (15 wt% loading).

(shown in Figure 6B). As it is shown in Figure 6B, it is clearly observed that thermal behavior of MMM is different compared to that of bare polymeric membrane. Interaction between MOF and polymer matrix is the reason for such change in behavior. MMMs are quite stable up to 270 °C with no significant weight loss. Next, they start initial degradation, which continues up to 380 °C where they undergo sharp degradation of polymer matrix, which continues until 410 °C resulting in a total loss of 70% of the initial weight. Afterward, they undergo comparative slow weight loss resulted from degradation of incorporated ZIF-94. Finally, weight loss ends at 570 °C with a residue of ≈5% of its initial weight. This residue roughly corresponds to ZnO generated (4.4 wt%) upon the thermal oxidation of the 15 wt% of MOF embedded in the MMM.

3.3.2. MMMs Performance

For membrane performance analysis, we focused on the four different types of fillers described in Table 3. Filler types ZIF-94 (1) and ZIF-94 (5) have very similar particle size differing but in BET SSA, hence the comparison of these two fillers will reveal the effect of BET SSA on membrane performance for CO_2 capture. ZIF-94 (product B) is a filler synthesized from the waste mother liquor of ZIF-94 (5). In this case, gas separation

performance comparison between ZIF-94 (5) and product B will reveal applicability of recycled ZIF-94 and potential differences in membrane performance. ZIF-94 (3) was MOF synthesized at higher pH (10) which will reveal information of the influence of the pH on membrane performance.

Polymer-Matrix Optimization: ZIF-94 Original Synthesis: MMMs were fabricated with two different polymer concentrations: 6 and 9 wt% Pebax MH 1657 as a matrix (i.e., the polymer concentration in the solvent as a casting solution) and various ZIF-94 (1) doses (5–20 wt%). These MMMs were analyzed for their performance over CO_2/N_2 mixture separation and compared with bare polymer membrane where error was calculated for two consecutive measurements with different membrane samples. The membrane thickness for was between 33 and 45 µm, and the CO_2 permeability as well as CO_2/N_2 selectivity for both polymer concentrations and different ZIF-94 loadings are presented in **Table 4** and **Figure 7**. Focusing first on the 6 wt% Pebax MH 1657, we have noticed that permeability increased by 200% (for MMM with 10 wt% fillers) compared to bare membrane due to the addition of ZIF-94 (1) filler (increment was calculated from Equation (4)). However, CO_2/N_2 selectivity was slightly lower compared to bare membrane for all compositions of 6 wt% Pebax MH 1657 MMMs, which implies there is a trade-off between both parameters

Table 4. Summary of the CO_2 capture performance of 6 wt% matrix based MMMs with ZIF-94 (1).

Polymer [wt%]	MOFs loading [wt%]	Average membrane thickness [µm]	Permeability [Barrer]	Selectivity (CO_2/N_2)
6	0	33 ± 7	43 ± 5	33 ± 2
	5	36 ± 5	100 ± 6	32 ± 3
	10	38 ± 8	126 ± 44	28 ± 5
	15	41 ± 7	106 ± 22	31 ± 3
	20	45 ± 3	96 ± 2	32 ± 2
9	0	40 ± 5	76 ± 7	21 ± 2
	5	42 ± 3	103 ± 24	32 ± 1
	10	45 ± 4	137 ± 31	36 ± 7
	15	46 ± 8	96 ± 11	31 ± 2
	20	46 ± 6	128 ± 27	26 ± 7

**ADVANCED
SCIENCE NEWS**

www.advancedsciencenews.com
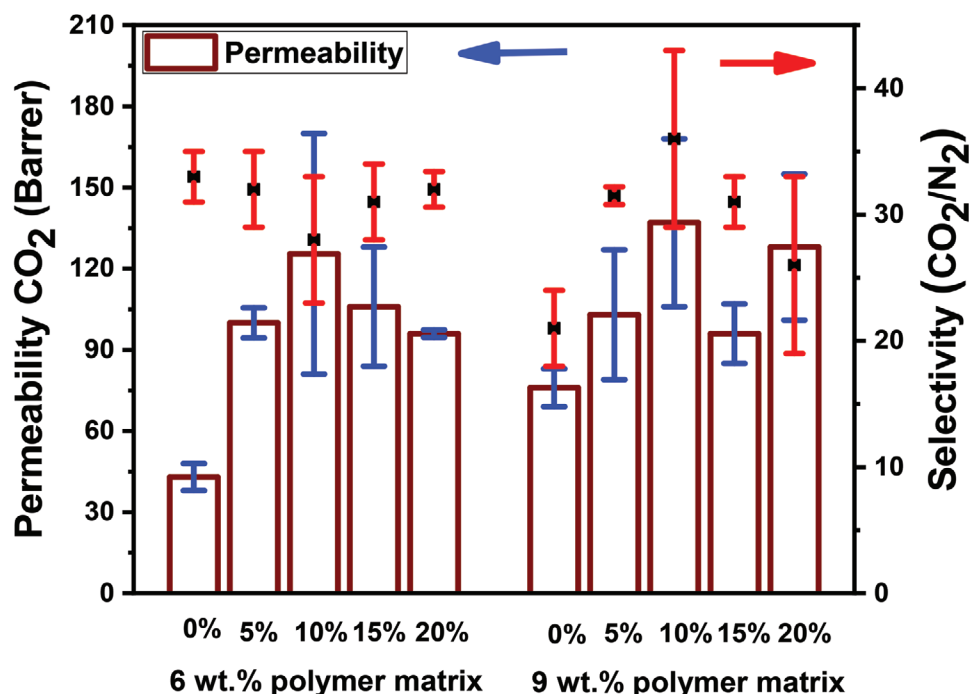
**ADVANCED
SUSTAINABLE
SYSTEMS**

www.advsustainsys.com

Figure 7. Performance of MMMs (6 and 9 wt% Pebax MH 1657 + various ZIF-94 (1) loadings).

$$\text{Improvement}\,(\%) = \frac{\begin{array}{c}\text{Performance of a membrane}\\-\text{Performance of bare membrane}\end{array}}{\text{Performance of bare membrane}} \times 100 \quad (4)$$

Moving to 9 wt% Pebax MH 1657, it was found that selectivity this bare membrane decreased significantly compared to 6 wt% bare membrane (see Figure 7 and Table 4). This trend is also reported by Martínez-Izquierdo et al.[31] The highest CO_2/N_2 selectivity of 36 ± 7 and the permeability of 137 ± 31 Barrer were obtained for 9 wt% Pebax MH 1657 based MMMs and 10 wt% loading of ZIF-94 (1). Comparison with bare membrane indicates that 10 wt% ZIF-94 (1) dose in the MMM increases selectivity and permeability by 71% and 80%, respectively. Further increase in MOF dose was found to decrease selectivity (CO_2/N_2) down to 26 ± 7 for 20 wt% filler content whereas the permeability did not change significantly (128 ± 27 Barrer). 15 wt% filler in 9 wt% polymer is another interesting composition which yields a mean permeability of 96 ± 11 Barrer with a CO_2/N_2 selectivity of 31 ± 2. It is also indicated that, inclusion of fillers (for all compositions) in the polymer matrix has produced considerable increase of both permeability and CO_2/N_2 selectivity by 120% and 105%, respectively. Which justifies that 9 wt% polymer matrix can be considered optimum composition to investigate the other three different types of ZIF-94. ZIF-94 improved the MMM performance due to its microporosity with pores of ≈0.26 nm,[35] favoring the diffusion of the smallest CO_2 molecule (0.33 nm of kinetic diameter versus 0.364 nm for N_2) in the mixture.[19] This is complemented with the improved CO_2 affinity of the MOF (better for ZIF-94 than for other typical ZIFs) due to its aldehyde functionalized ligand.[36,37]

Effect of Different ZIF-94 Fillers on the Membrane Performance: Further investigation on the optimum matrix composition

(9 wt% polymer matrix) was carried out for other three different types of MOFs: (ZIF-94 (5), product B, and ZIF-94 (3)), with loadings variation of 5, 10, and 15 wt%, which are represented in **Figure 8**. Investigation on ZIF-94 in 9 wt% polymer-based MMMs represents that CO_2 permeability increases for all compositions of MMMs (for all four different ZIF-94 fillers) compared to bare polymeric membrane. As expected, 10 wt% of ZIF-94 (5) loading resulted in the highest selectivity of 32 ± 2 and permeability of 125 ± 12 Barrer, which represent 52% and 65% increments, respectively, when compared with bare membrane. Moreover, the conducted measurements showed a decreasing tendency for both selectivity and permeability on further increase of the filler in MMMs. The investigation on product B, which was recycled from waste mother liquor of ZIF-94 (5), revealed that permeability can be improved compared to bare membrane for all composition filler dose being used but CO_2/N_2 selectivity surpassed the bare membrane only in case of 10 wt% filler dose. A similar response was found for ZIF-94 (3) when it was incorporated inside MMMs and examined for CO_2 analysis. From the discussion so far, it can be considered that 10 wt% filler is the optimum loading for 9 wt% Pebax MH 1657 based MMMs. Robeson upper bound plot is presented in Figure S7 of the Supporting Information with performance of the MMMs under investigation. Additionally, gas separation performances of the membranes are listed in Table S3 of the Supporting Information.

Comparison of two different fillers (ZIF-94 (1) and ZIF-94 (5)) possessing similar average particle sizes but different BET SSA (317 and 457 m² g⁻¹, respectively, see Table 3) demonstrated the effect of this textural parameter on the CO_2 capture. It is clearly evidenced that both fillers produced different responses when incorporated into MMMs at optimum concentration (i.e., 10 wt%). More importantly there were improvements by 10%
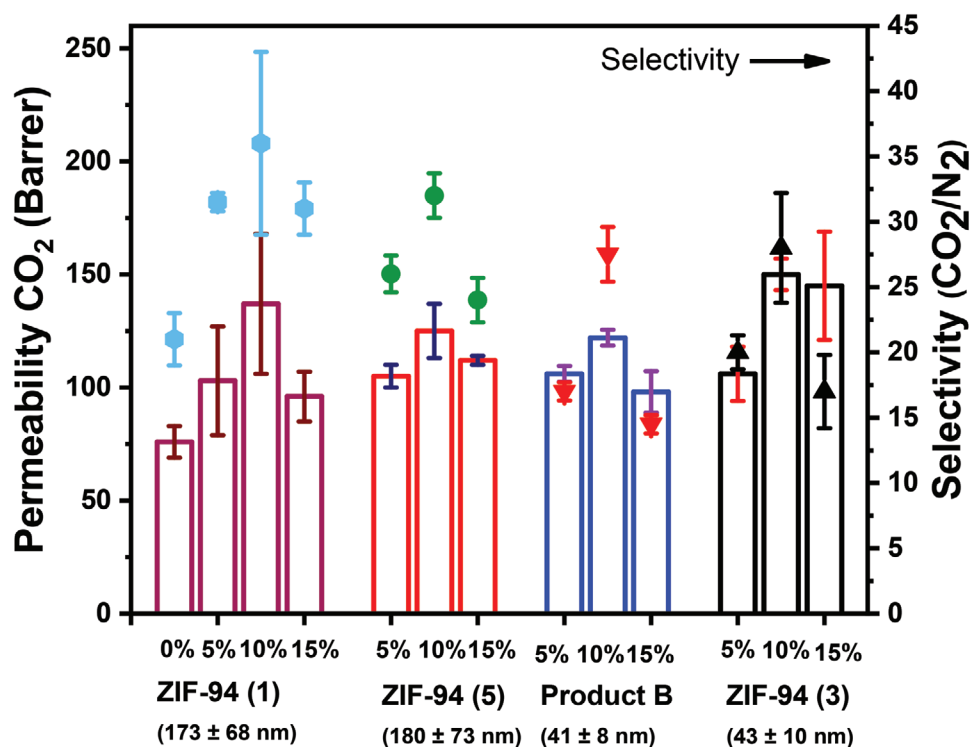
Figure 8. Performance of MMMs at 9 wt% of Pebax MH 1657 with different types of ZIF-94.

and 11% for permeability and selectivity, respectively, due to higher BET SSA. In the further observation, recycled ZIF-94 (i.e., product B) with mean particle size of 41 ± 8 nm and fresh ZIF-94 (5) possessing an average particle size of 180 ± 73 nm produced different performance on CO_2 capture (see Figure 8). Best CO_2/N_2 selectivity of freshly synthesized filler at 10 wt% filler loading is 32 ± 2 which is 14% higher than in case of recycled product B, being equal to 28 ± 2. Whereas selectivity for 5 and 15 wt% loadings are significantly lower than that of the bare polymer membrane. This allows one to partially conclude that the recycled mother liquor filler may improve, at the best optimum loading, the MMM performance of the bare polymer. Nonetheless, the particle size shows an important effect on the MMM performance which has been already reported for MMMs containing ZIF-8 where they explained that, fillers agglomeration tendency may prevent the smallest MOFs nanoparticles to constitute the best MMMs.[38] In addition, this suggests that additional synthesis work is needed to control the particle size of ZIF-94 when prepared from recycled mother liquors.

A comparison between recycled and fresh MOF pairs product B and ZIF-94 (3) with almost identical particle size (41 ± 8 nm nm and 43 ± 10, respectively) was conducted (see Figure 8). Only optimum filler composition (that is 10 wt%) surpasses the limit of bare membranes in terms of both selectivity and permeability. Confirming the suitability of mother liquor recycle to obtain ZIF-94 as filler for MMMs, both fillers produce similar selectivity of 28, whereas freshly synthesized ZIF-94 (3) showed 23% additional increase in permeability (that is 150 ± 6 Barrer) compared to recycled product B, which resulted in 122 ± 4 Barrer. Comparison of all the fillers at the

optimum concentration of 10 wt% is represented in **Figure 9**. It is evidenced that higher selectivity is attainable for fillers having bigger particle size. Whereas smaller particles produce higher permeability with some extend of sacrificial selectivity. A maximum increase in permeability (100% increase) has been found for ZIF-94 (3) which has particle size of 43 ± 10 nm. Figure 9 also suggests a better reproducibility in the separation performance (smaller error bars) for the MMM prepared from the pH controlled synthesis as compared to the parent ZIF-94 synthesis. On the other hand, highest increment in average selectivity (71%) was obtained for ZIF-94 (1) which possesses average
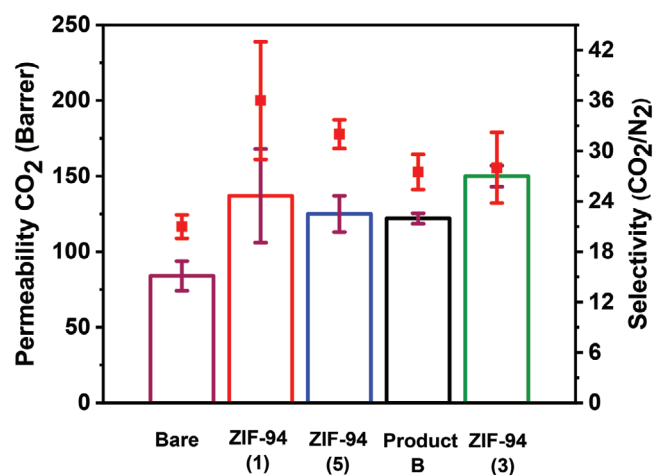

Figure 9. Effect of different ZIF-94 fillers for MMMs 9 wt% Pebax MH 1657 on CO_2 capture at the optimum filler composition (10 wt%).

particle size of 173 ± 68 nm. Recycled product B also complies with the performance of freshly synthesized ZIF-94 (3). This confirms the reuse of waste mother liquor as a green practice to reduce the chemical loss in the MOF synthesis and thus minimize the impact of the MMM preparation on the environment.

Moreover, it was noticed that there is a correlation between membrane thickness and permeability. Permeability through MMMs is linearly proportional to the membrane thickness. Produced results also found to be reproducible with some error. According to the literature, Selyanchyn et al. have reported that CO_2 permeability through bare Pebax MH 1657 membrane increases up to 140 Barrer at 80 µm membrane thickness. It was reported by the authors that further increase of membrane thickness reduces CO_2 permeability down to 110 Barrer for 128 µm thickness.[39] In this research, MMMs membrane with thickness of 37 µm produces CO_2 permeability of 122 Barrer which increases up to 150 Barrer for membrane thickness of 47 µm.

Finally, Figure S8 and Table S4 of the Supporting Information show a comparison of the best separation performances in this work with the state-of-the-art MMM benchmarks using as a filler typical ZIFs. It is observed that the data presented in Figure S8 of the Supporting Information follow the general trade-off between CO_2/N_2 selectivity and CO_2 permeability. The membranes of this work show good performance. It should be considered that one of the represented membranes comes from a ZIF-94 obtained from a recycled mother liquor, which indicates that it is possible to improve the preparation of the MMMs from a more economic and environmental point of view reducing significantly their performance.

4. Conclusions

In this work, the initial synthesis and methodology developed to produce ZIF-94 nanocrystals from the recycling of its mother liquors were carried out. Two main synthesis parameters were modified: pH and temperature. In all the conditions investigated pure, crystalline ZIF-94 was obtained. The most promising results, taking into account crystallinity, yield of the reaction and BET specific surface area, were obtained when both, the initial synthesis (BET: 463 m^2 g^{-1}, particle size: 43 nm) and the mother liquor (product A.4; BET: 483 m^2 g^{-1}; particle size: 34 nm), were carried out at pH = 10.

After the successful synthesis of ZIF-94 from the recycled mother liquors, the fabrication of a defect-free mixed matrix membrane with Pebax MH 1657 as a continued phase and synthesized ZIF-94 as a dispersed phase was successfully conducted. ZIF-94 fillers obtained at different conditions with different particle sizes and slightly different BET specific surface area values were incorporated inside the polymeric membrane and the resulted MMMs were applied for the CO_2/N_2 separation. The optimum composition of MMMs was found to be 9 wt% Pebax MH 1657 and 10 wt% ZIF-94 loading. ZIF-94 of ≈180 in particle size was found to be the best filler in terms of selectivity 36 ± 7 and permeability 137 ± 31 Barrer, whereas ZIF-94 of ≈40 nm produced maximum permeability of 150 ± 7 Barrer (with selectivity of 28 ± 4). This suggests that particle agglomeration of the filler may affect the separation

performance, in line with previous reports with analogous ZIFs. In conclusion, additional synthesis improvement is needed to control the particle size of ZIF-94 when preparing it from recycled mother liquors, and fabricated membranes were found to be stable at the operating condition since no damage, cracks or nonselective gaps in the membrane was observed.

Supporting Information

Supporting Information is available from the Wiley Online Library or from the author.

Conflict of Interest

The authors declare no conflict of interest.

Data Availability Statement

The data that support the findings of this study are available from the corresponding author upon reasonable request.

[1] H. Yang, Z. Xu, M. Fan, R. Gupta, R. B. Slimane, A. E. Bland, I. Wright, *J. Environ. Sci.* **2008**, *20*, 14.

[2] Z. Dai, R. D. Noble, D. L. Gin, X. Zhang, L. Deng, *J. Membr. Sci.* **2016**, *497*, 1.

[3] A. Tellez-Rio, A. Vallejo, S. García-Marco, D. Martin-Lammerding, J. L. Tenorio, R. M. Rees, G. Guardia, *Eur. J. Agron.* **2017**, *84*, 95.

[4] K. Xie, Q. Fu, G. G. Qiao, P. A. Webley, *J. Membr. Sci.* **2019**, *572*, 38.

[5] W. J. Choi, J. B. Seo, S. Y. Jang, J. H. Jung, K. J. Oh, *J. Environ. Sci.* **2009**, *21*, 907.

[6] L. M. Robeson, *J. Membr. Sci.* **2008**, *320*, 390.

[7] H. C. Zhou, J. R. Long, O. M. Yaghi, *Chem. Rev.* **2012**, *112*, 673.

[8] M. Anson, J. Marchese, E. Garis, N. Ochoa, C. Pagliero, *J. Membr. Sci.* **2004**, *243*, 19.

[9] M. Shah, M. C. McCarthy, S. Sachdeva, A. K. Lee, H. K. Jeong, *Ind. Eng. Chem. Res.* **2012**, *51*, 2179.

**ADVANCED
SCIENCE NEWS**

www.advancedsciencenews.com

**ADVANCED
SUSTAINABLE
SYSTEMS**

www.advsustainsys.com

[10] S. Aguado, J. Canivet, D. Farrusseng, *Chem. Commun.* **2010**, *46*, 7999.

[11] N. Keser Demir, B. Topuz, L. Yilmaz, H. Kalipcilar, *Microporous Mesoporous Mater.* **2014**, *198*, 291.

[12] W. Morris, N. He, K. G. Ray, P. Klonowski, H. Furukawa, I. N. Daniels, Y. A. Houndonougbo, M. Asta, O. M. Yaghi, B. B. Laird, *J. Phys. Chem. C* **2012**, *116*, 24084.

[13] J. Canivet, J. Bonnefoy, C. Daniel, A. Legrand, B. Coasne, D. Farrusseng, *New J. Chem.* **2014**, *38*, 3102.

[14] A. Sabetghadam, X. Liu, M. Benzaqui, E. Gkaniatsou, A. Orsi, M. M. Lozinska, C. Sicard, T. Johnson, N. Steunou, P. A. Wright, C. Serre, J. Gascon, F. Kapteijn, *Chem. - Eur. J.* **2018**, *24*, 7949.

[15] T. Zhou, Y. Sang, X. Wang, C. Wu, D. Zeng, C. Xie, *Sens. Actuators, B* **2018**, *258*, 1099.

[16] S. Lazare, D. Bazer-bachi, F. Bonnier, E. Soyer, A. Quoineaud, N. Bats, *J. Am. Chem. Soc.* **2010**, *132*, 12365.

[17] M. Etxeberria-Benavides, O. David, T. Johnson, M. M. Łozińska, A. Orsi, P. A. Wright, S. Mastel, R. Hillenbrand, F. Kapteijn, J. Gascon, *J. Membr. Sci.* **2018**, *550*, 198.

[18] F. Cacho-Bailo, I. Matito-Martos, J. Perez-Carbajo, M. Etxeberría-Benavides, O. Karvan, V. Sebastián, S. Calero, C. Téllez, J. Coronas, *Chem. Sci.* **2017**, *8*, 325.

[19] A. Noguera-Díaz, J. Villarroel-Rocha, V. P. Ting, N. Bimbo, K. Sapag, T. J. Mays, *J. Chem. Technol. Biotechnol.* **2019**, *94*, 3787.

[20] N. Tannert, S. Gökpinar, E. Hastürk, S. Nießing, C. Janiak, *Dalton Trans.* **2018**, *47*, 9850.

[21] S. Gökpinar, T. Diment, C. Janiak, *Dalton Trans.* **2017**, *46*, 9895.

[22] M. García-Palacín, J. I. Martínez, L. Paseta, A. Deacon, T. Johnson, M. Malankowska, C. Téllez, J. Coronas, *ACS Sustainable Chem. Eng.* **2020**, *8*, 2973.

[23] N. Jamil, N. H. Alias, M. Z. Shahruddin, N. H. Othman, *Key Eng. Mater.* **2019**, *797*, 48.

[24] F. Şahin, B. Topuz, H. Kalıpçılar, *Microporous Mesoporous Mater.* **2018**, *261*, 259.

[25] Q. Shi, Z. Song, X. Kang, J. Dong, Y. Zhang, *CrystEngComm* **2012**, *14*, 8280.

[26] S. R. Venna, J. B. Jasinski, M. A. Carreon, *J. Am. Chem. Soc.* **2010**, *132*, 18030.

[27] X. Gong, Y. Wang, T. Kuang, *ACS Sustainable Chem. Eng.* **2017**, *5*, 11204.

[28] J. Yuan, H. Zhu, J. Sun, Y. Mao, G. Liu, W. Jin, *ACS Appl. Mater. Interfaces* **2017**, *9*, 38575.

[29] D. Madhav, M. Malankowska, J. Coronas, *New J. Chem.* **2020**, *44*, 20449.

[30] T. Johnson, M. M. Łozińska, A. F. Orsi, P. A. Wright, S. Hindocha, S. Poulston, *Green Chem.* **2019**, *21*, 5665.

[31] L. Martínez-Izquierdo, M. Malankowska, J. Sánchez-Laínez, C. Téllez, J. Coronas, *R. Soc. Open Sci.* **2019**, *6*, 190866

[32] A. S. Embaye, L. Martínez-Izquierdo, M. Malankowska, C. Téllez, J. Coronas, *Energy Fuels* **2021**, *35*, 17085.

[33] Z. Su, Y. R. Miao, G. Zhang, J. T. Miller, K. S. Suslick, *Chem. Sci.* **2017**, *8*, 8004.

[34] A. M. Marti, M. Van, K. J. Balkus, *J. Porous Mater.* **2014**, *21*, 889.

[35] A. Sabetghadam, X. Liu, M. Benzaqui, E. Gkaniatsou, A. Orsi, M. M. Lozinska, C. Sicard, T. Johnson, N. Steunou, P. A. Wright, C. Serre, J. Gascon, F. Kapteijn, *Chem. - Eur. J.* **2018**, *24*, 7949.

[36] F. Cacho-Bailo, G. Caro, M. Etxeberría-Benavides, O. Karvan, C. Téllez, J. Coronas, *RSC Adv.* **2016**, *6*, 5881.

[37] K. G. Ray, D. L. Olmsted, J. M. R. Burton, Y. Houndonougbo, B. B. Laird, M. Asta, *Chem. Mater.* **2014**, *26*, 3976.

[38] J. Sánchez-Laínez, B. Zornoza, S. Friebe, J. Caro, S. Cao, A. Sabetghadam, B. Seoane, J. Gascon, F. Kapteijn, C. L. Guillouzer, G. Clet, M. Daturi, C. Téllez, J. Coronas, *J. Membr. Sci.* **2016**, *515*, 45.

[39] R. Selyanchyn, M. Ariyoshi, S. Fujikawa, *Membranes* **2018**, *8*, 121.